Robust uncertainty quantification of the volume of tsunami ionospheric holes for the 2011 Tohoku-Oki Earthquake: towards low-cost satellite-based tsunami warning systems

Ryuichi Kanai[1], Masashi Kamogawa[3], Toshiyasu Nagao[4], Alan Smith[2], Serge Guillas[1]

[1]Department of Statistical Science, University College London, London, UK
[2]Department of Space and Climate Physics, University College London, London, UK
[3]Global Center for Asian and Regional Research, University of Shizuoka, Shizuoka, Japan
[4]Institute of Oceanic Research and Development, Tokai University, Shizuoka, Japan

Key Points:

- First estimation of volumes of tsunami ionospheric holes, tracking the Global Navigation Satellite System.
- Tsunami ionospheric holes surfaces and their uncertainties are determined every 30 s from moving observations.
- Confident detection of tsunamis is enabled within 15 minutes for Japan and likely any source worldwide.

Corresponding author: Ryuichi Kanai, ryuichi.kanai.16@ucl.ac.uk

Abstract

We develop a new method to analyze the total electron content (TEC) depression in the ionosphere after a tsunami occurrence. We employ Gaussian process regression to accurately estimate the TEC disturbance every 30 s using satellite observations from the GNSS network, even over regions without measurements. We face multiple challenges. First, the impact of the acoustic wave generated by a tsunami onto TEC levels is nonlinear and anisotropic. Second, observation points are moving. Nevertheless, our method always computes these volumes, along with estimated uncertainties, when applied to the 2011 Tohoku-Oki Earthquake, even with random selections of only 5% of the 1,000 GPS Earth Observation Network System receivers considered here over Japan. The method can warn of a tsunami event within 15 minutes of the earthquake, at high levels of confidence, even with a sparse receiver network. Hence, it is potentially applicable worldwide using the existing GNSS network.

Plain Language Summary

The air above the tsunami source is compressed by the locally raised sea surface. That increase in air pressure propagates upwards and causes a depression in the electron density in the upper atmosphere, which is related to the size of the initial tsunami. The physical mechanisms involved are complex. Variations in electron density in the upper atmosphere are detected from GPS satellite timing data but the interpretation is a challenge because the locations of the measurements from the satellites are moving. Nevertheless, our statistical method has made it possible to properly assess the volume (with uncertainties) of the electron density depression. An advantage of our technique is that it can estimate values even for regions where no measurement exist. Also, even when only 5% of the observed data were used, the phenomenon can be measured very accurately. When applied to the 2011 Tohoku-Oki Earthquake in Japan, our method makes it possible to warn of a tsunami event within 15 minutes of the earthquake. It is hoped, in the future, that this method will be embedded in early warning systems for tsunamis worldwide.

1 Introduction

The damage caused by tsunamis can be devastating. For example, more than 20,000 people died in the tsunami following the 2011 Tohoku tsunami in Japan. One reason for

such levels of casualties is that current tsunami height predictions are relatively unreliable, even following an identified earthquake event, and so early warning systems are not as effective as required. Initial sea surface deformations are typically indirectly determined from seismological inversions of the earthquake source. However, some of these early estimates are sometimes much lower than expected: for instance the 2011 Tohoku-oki earthquake initial estimated value of M_w7.9 was used for warnings but the actual magnitude was M_w9.1.

Furthermore, the initial tsunami wave cannot be precisely inferred from seismic information alone due to the complexity of the relationship between the earthquake source and the initial wave. For example so-called tsunami earthquakes generate much larger tsunamis than expected from the seismic source, e.g. the Mentawai 2010 tsunami (Lay et al., 2011; Satake et al., 2013), whereas some powerful earthquakes sometimes produce tsunamis much smaller than expected e.g. for the 2005 M_w8.6 Nias earthquake. These deficiencies in the seismic approach become even greater when considering additional contributions to the tsunami wave such as splay faults and submarine landslides not well picked up by seismic monitoring. One could account for the uncertainties in the earthquake source estimates and propagate these to the initial tsunami height in real-time (Giles et al., 2021), but these approaches cannot realistically model in 3-D and in real-time the seabed deformation arising from the earthquake source due to epistemic, computational and observational inadequacies. Hence, observations closely related to the actual generated tsunami wave are more likely to provide more precise warnings. One example is the successful data assimilation of tsunami wave from buoys, with either dense or possibly sparse networks (Tanioka & Gusman, 2018; Wang et al., 2019). We explore here the use of real-time satellite data due to its global coverage, low expense, low maintenance, and rapid access.

A path towards accurate warnings is to estimate the Tsunami Ionospheric Holes (TIHs) generated in the ionosphere after the initial tsunami occurrence (Kamogawa et al., 2016). The formation of a TIH, which is a decrease in total electron content (TEC) in the ionosphere, can be explained by the following physical mechanisms (Kamogawa et al., 2016; Shinagawa et al., 2013). First, a displacement of sea surface caused by a tsunami generates acoustic waves that propagate vertically upward and reach the ionosphere. Then, the plasma is moved along the magnetic field by the sound waves and the downward flow is larger than the upward flow partly because the gravity force causes downward motion.

The downward plasma causes recombination and ion production is suppressed, resulting in a decrease in TECs, and the depression in TECs is called a TIH. The TIH observed in the ionosphere at the time of the 2011 Tohoku tsunami has been reproduced by performing numerical simulations of this physical phenomenon (Shinagawa et al., 2013; Zettergren et al., 2017; Zettergren & Snively, 2019).

In Japan, the GPS Earth Observation Network System (GEONET), which is a network of more than 1,200 receivers, enables us to observe the behavior of the TEC in the ionosphere with a large number of data points. The most prominent case of the TEC changes in the ionosphere observed by GEONET is the tsunami following the 2011 Earthquake, off of the Pacific coast of Tohoku. By focusing on the changes in the ionosphere after the earthquake and observing the high-frequency component of the TEC fluctuations, Tsugawa et al. (2011) observed a rapid decrease in TEC near the epicenter approximately 7 minutes after the earthquake : the rapid fluctuation of the high-frequency component of TEC was detected as concentric waves that radiated outward, and these concentric waves were confirmed to have had a central point source. A. Saito et al. (2011) analyzed the unfiltered TEC fluctuations in which, a significant decrease in TEC was observed, with an amplitude of up to 5 TECu and an area of 500 km. Similarly, Kakinami et al. (2012) showed that the amplitude of the decrease in TEC exceeds 5 TECu, analyzing the TEC without frequency filtering.

Furthermore, Kamogawa et al. (2016) examined the behavior of the TEC depression in the ionosphere after the tsunami, examining the low-frequency component of TEC in a variety of tsunami cases including the 2011 Tohoku tsunami. They discovered a positive correlation between the initial tsunami height and the rate of TEC depression. It is thus likely possible to detect an initial tsunami by evaluating the magnitude of TIH, which is the reduction of the TEC in the ionosphere. However, it is still challenging to define the scale of TIH, because even if a dense network of GNSS receivers is maintained, such as in Japan, there are areas where the TEC cannot be measured by the network. Moreover, the TEC measurement locations move in the same way as the satellite moves, and those locations are not uniformly distributed within the target range. The shape of the TIH cannot be completely captured from the measurement points alone. In addition, in regions where GNSS observation networks are less dense, the number of available data is even smaller, making it very difficult to detect the TIH confidently.

To overcome these problems, we implement below a statistical method for the analysis of TEC using satellite data, which allows us to estimate TEC values even over areas with no measurements and even to evaluate the whole TIH even without a dense measurement network such as GEONET in Japan. Our approach does not make any assumption on the nature of the source of the tsunami. This method enables us to calculate the volume (with uncertainty) of the hole as an assessment of the scale of the TIH, and we propose to use its volume as a measure of the TIH. We believe that estimating the TIH provides a new and important tool for early tsunami warning systems that is independent of seismology.

In section 2, the pre-processing and characteristics of the data are described in detail to ensure that this study is reproducible. In addition, we describe our surface fitting method. In section 3, we present the results of fitting surfaces computed by our new method and the time series analysis of the TIH volume. In section 4, we conclude and mention future possibilities offered by this method.

2 Data and Method

2.1 Data

In this study, TEC is calculated using GEONET data operated by the Geospatial Information Authority of Japan, and the following assumptions are made in processing the data. First, we approximate the F region, which contains many more electrons than other regions in the ionosphere, as a thin layer at an altitude of 300 km because the two effects of the chemical reactions and diffusion are balanced and the electron density is maximized at an altitude of 300 km. The point where the line connecting a GNSS satellite and a receiver intersects with this approximated thin layer is called the ionospheric point (IP). The footprint of the IP to the surface is called the Sub-Ionospheric Point (SIP).

Two radio signals from the GNSS satellites, 1575.42 MHz and 1222.60 MHz, are transmitted to the GNSS receivers, and the propagation time of the radio signals depends on the electron density in the atmosphere. Therefore, the TEC between the GNSS satellites and the GNSS receivers can be estimated from the phase delay of these two types of radio signals. This TEC, which is in the pathway between a satellite and a receiver, is called the slant TEC, noting that in general the line of sight to the satellite is not vertical. The slant TEC at the time of the earthquake is used as the reference value for the

time-series slant TEC data. The time-series slant TEC is defined as the difference between the slant TEC and the reference TEC value for each satellite receiver pair.

For each time-series slant TEC data, a quadratic fitting is performed by the ordinary least-squares method for data points from 30 minutes before to 7 minutes after the time of the earthquake to be consistent with the previous study (Kamogawa et al., 2016). These fitting curves are assumed to represent the time series slant TEC data as it would have been in the absence of the effect of TEC depression caused by acoustic waves induced by the tsunami because it takes almost 7 minutes for acoustic waves to reach the ionosphere.

Then, we calculate the difference between the fitting curves and the time-series slant TECs for each case. By multiplying the time series differences by the cosine of the angle θ between the vertical upward direction and the straight line between the satellite and the receiver, we obtain ΔvTEC, which is the variation of the vertical component of the slant TEC time series data. The conceptual diagram of the description of the data processing so far is drawn in Figure 1.

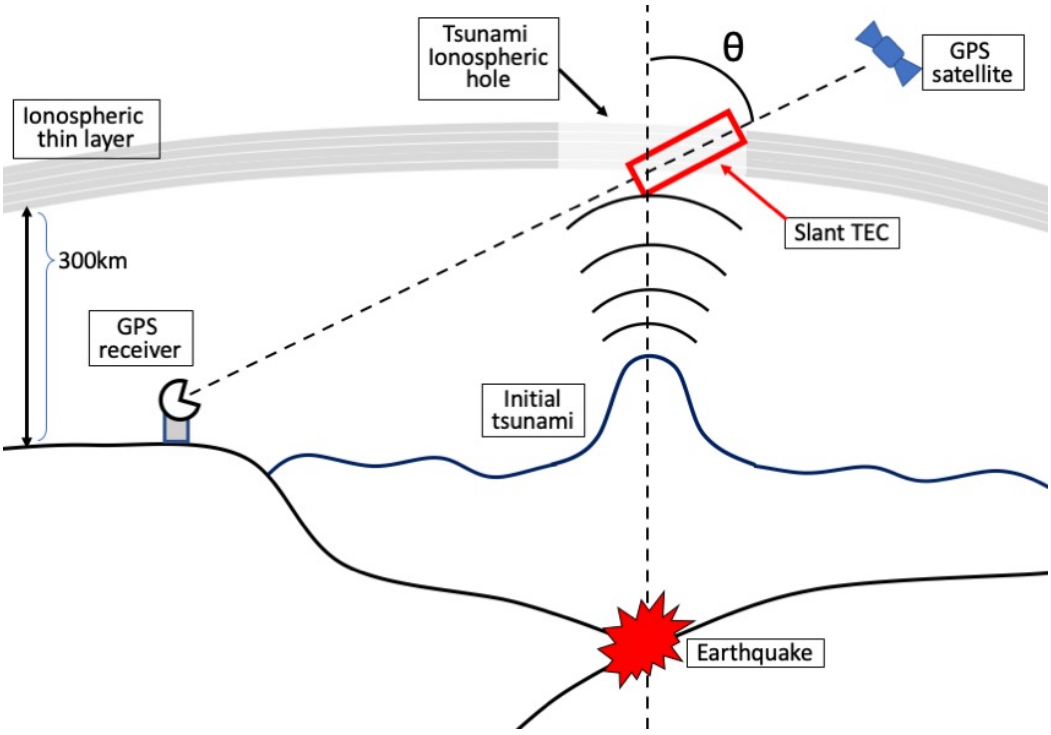

Figure 1. The schematic image of TEC depression detected by a satellite and a receiver.

To apply a low-pass filter to this ΔvTEC, we take a 300 seconds backward moving average to obtain the low-frequency components of ΔvTEC. Since TIH is a hole formed by the decrease of TEC, we want to focus on the decrease of TEC in our analysis. For this reason, in the following sections, we use the data of which the low-frequency ΔvTEC is less than 1. The low-frequency ΔvTEC is hereinafter referred as TEC for sake of simplicity.

The unit of TEC is TECu, which is 1.0×10^{16}electron m^{-2}. Since the time resolution of the available data is the 30-second interval, we set the time of the 2011 off the Pacific coast of Tohoku Earthquake occurrence as 6:46:30 UTC even though the exact occurrence time is 6:46:18 UTC according to the Japan Meteorological Agency. In addition, the data include outliers due to broken receivers, so we detected them using a method based on K-nearest neighbor algorithm (Cover & Hart, 1967), and removed these outliers from the data to be analyzed.

2.2 Robust Fitting Method with Gaussian Process Regression

We analyse data over the area of 10 degrees of latitude and 10 degrees of longitude centered at 38.297°N and 142.373°E, the location of the epicenter of the 2011 Tohoku Earthquake as reported by the USGS, see Figure 2. Gaussian process (GP) regression (Williams & Rasmussen, 2006) is a method of regressing a function Y (here the TEC as a function of horizontal coordinates) using a flexible nonlinear model based on a set of observed data. A GP is in fact a generalization of the multivariate normal distribution to infinite dimensions: any marginal distribution projected to finite dimensions is multivariate normal. The fitted GP here probabilistically represents all possible TEC surfaces that interpolate (up to a so-called nugget noise level) the observations. We employ here the Matérn kernel with an additional nugget that accounts for some noise about the observations:

$$k_\nu(\boldsymbol{x_p}, \boldsymbol{x_q}) = \frac{2^{1-\nu}}{\Gamma(\nu)}\left(\frac{\sqrt{2\nu}r}{l}\right)^{\nu} K_\nu\left(\frac{\sqrt{2\nu}r}{l}\right), \qquad \text{where } r = |\boldsymbol{x_p} - \boldsymbol{x_q}| \tag{1}$$

$$cov(y_p, y_q) = k_\nu(\boldsymbol{x_p}, \boldsymbol{x_q}) + \sigma^2\delta_{p,q} \tag{2}$$

Here, K_ν is a modified Bessel function of the second kind, Γ is the Gamma function, ν and l are positive parameters, σ^2 is the variance of the noise (i.e. the nugget), and $\delta_{p,q} = 1$ if $p = q$ and zero otherwise. The Matérn Kernel's smoothness ν generates a GP whose smoothness relates to ν, and should thus be carefully chosen to match the smoothness

of the function Y. By setting $\nu = 5/2$, we use a kernel function that is twice differentiable, which, in our analysis, conforms very well to the physical phenomena of TEC reduction.

After fitting our GP, the joint distribution of the estimates at any new locations are estimated (with uncertainty) even in areas where there is no measurement data. Here we predict the TEC surface over the area in increments of 0.01 degrees in both latitude and longitude. However, using 1,200 receivers, it takes more than 10 minutes to fit the full data due to costs of $\mathcal{O}(n^3)$ where n is the number of data points.

A stochastic partial differential equation (SPDE) approach using the integrated nested Laplace approximation (INLA) (Lindgren et al., 2011; Rue et al., 2009) can reduce the cost of fitting the GP. Such an approach not only is faster but has demonstrated that spatial predictions are more accurate, less uncertain and more robust than the standard covariance-based fitting of a GP e.g. when mapping stratospheric ozone (Chang et al., 2015). Exploiting Gaussian Markov random fields (GMRF), INLA-SPDE reduces costs to $\mathcal{O}(n^{\frac{3}{2}})$ for two dimensions. The crucial point is that a Gaussian spatial process with a Matérn covariance function is the stationary solution to a certain SPDE that can be solved using finite element approaches and approximated using the INLA in the GMRF setting. Nevertheless, some effort must be put into creating a reasonable mesh that solves the SPDE using finite elements, shown in Figure S1 in the supporting information for our region. The number of elements in the mesh cannot be too large as the computational burden would become too high, and not too small, as the surface would not be a good approximation of the actual surface.

Using this INLA-SPDE method with about 5,200 mesh elements, the average computational time to fit the full data and predict the surface in 30-second increments from 5:30:00 to 6:30:00 becomes less than 1 minute, with a standard deviation of less than 5 seconds, whereas the average computational time based on the standard GP regression method is more than 10 minutes, with a standard deviation of more than 2 minutes.

3 Results

The absolute values of the outliers can reach over 50 TECu, which can distort the fitting surface considerably. Therefore, all the analysis in this study are implemented after removing the outliers.

Figure 2 shows that measured TEC data, its surface fitting, and 2D mapping for both full data and sparse data. Although Figure 2 panel (a) shows that the observed TEC decreases near the epicenter, the position where it decreases the most and the range of depression cannot be described in detail due to the limited number of data points.

However, panels (c), (e), and (g) show that the surface fitting enables us to estimate the TEC values with uncertainty even over the region where the data is not detected by the GNSS satellites and receivers. The estimated values are displayed in increments of 0.01 degrees in latitude and longitude.

The panel (b) shows the TEC data measured by only 5% of the receivers chosen at random. The surface fitting method works effectively and succeeds in capturing the TIH using the sparse data as shown in the panel (d) and (f). It can also be seen that the uncertainty increases with a smaller number of data points. The panel (h) shows that even with sparse data, the location and range of the TIH is adequately estimated and consistent with the case of full data shown in the panel (g). For more details, the time series movies of each panel in Figure 2 in the supporting information.

Figure 3 shows the measured TEC data at different times and the time series of the TIH volume, which is calculated by trapezoidal quadrature method for the region where the TEC estimated by the surface fitting has a negative value. In other words, the volume between the flat surface, that is the TEC values are equal to 0, and the fitting surface is calculated. In panels (a), (b), (c), and (d), the red star is the location of the epicenter of the 2011 Tohoku Earthquake and the two large black circles with slanting lines are outliers, which are excluded using our method.

The main effect by acoustic waves induced by the initial tsunami is that the reduction of TEC by moving the plasma along the magnetic field and causing recombination. More specifically, although there are regions where the TEC increases due to complex physical mechanisms, the magnitude of the initial tsunami can be assessed by focusing on the decrease in the TEC. Therefore, the volume of the region with negative TEC value is considered to be related to the magnitude of the initial tsunami.

The solid lines in the panel (e) and (f) in Figure 3 display the TIH volumes computed for the full data and the dashed lines are for the sparse data. In the case of the sparse data, we repeat 10 times the randomly selection of 5% of the receivers and the Gaussian process regression to fit the surfaces, and then calculate the average value of the resulting volume. This iterative process excludes a possible influence of the random

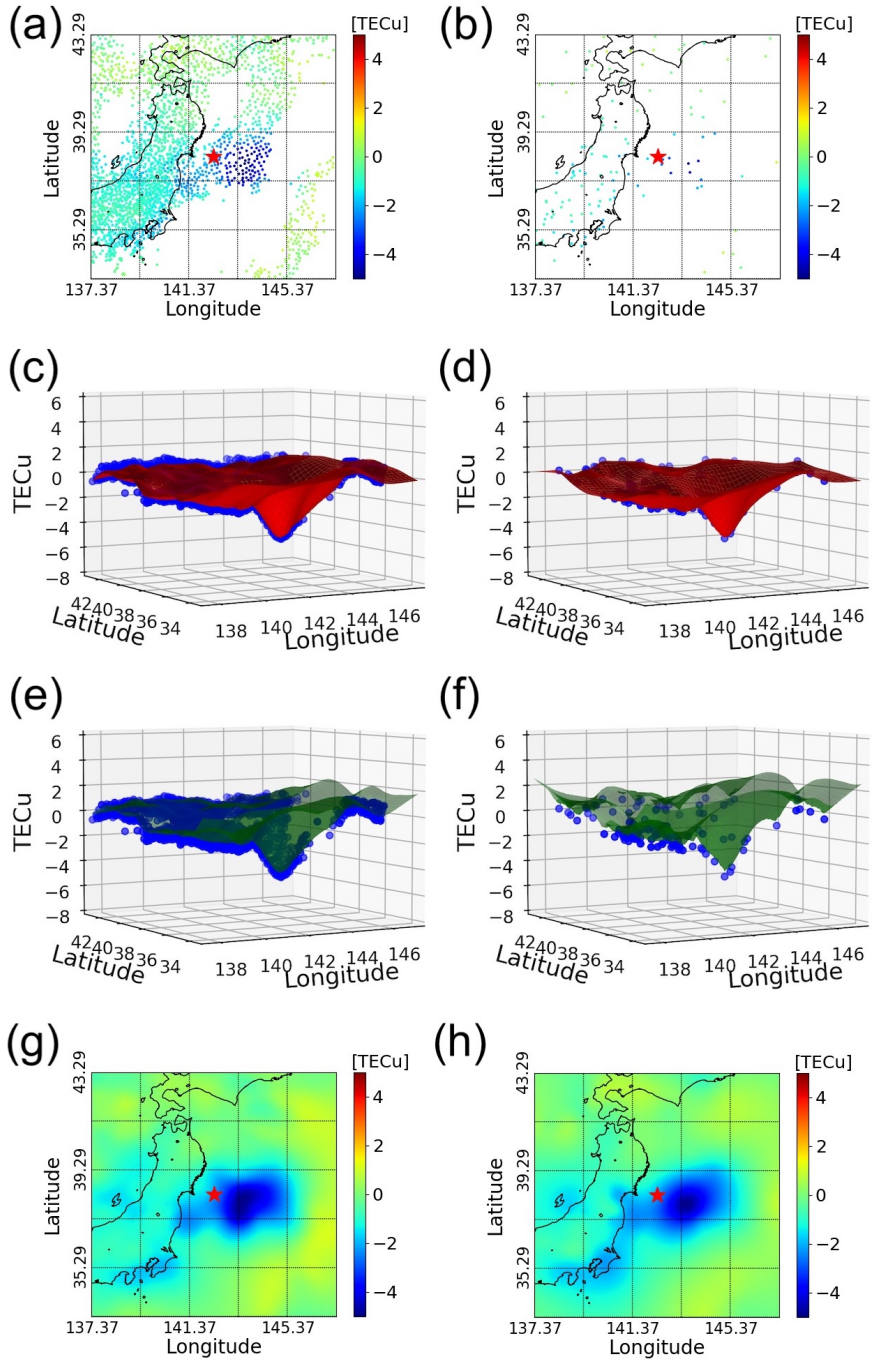

Figure 2. Left-hand side is for the full data and right-hand side is for the sparse data using only 5% of the GEONET receivers. (a) and (b) are measured TEC data. (c) and (d) are measured TEC data (blue dots) and the fitting surface (red surface). (e) and (f) are measured TEC data (blue dots) and 99% one-sided confidence interval of the fitting surface (green surface). (g) and (h) are 2D projection of the fitting surface. All plots are for data at 6:08:30 (UCT). The fitting surface is computed using the INLA-SPDE method.

seed used in the sparse data selection on the results. As shown in the panel (a), (b), (c), and(d), the measurement points are moving and not uniformly distributed in the targeting range. Still, the time series of the computed TIH volumes looks continuous, as shown in the panel (e) and (f).

The warning system based on this method is highly feasible because the surface fitting and the estimation of the TEC values for the full data can be processed in less than a minute based on the INLA-SPDE method. However, in the case of the sparse data fitting, our implementation of the INLA-SPDE method sometimes fails due to the geometric meshing optimised for larger data sets, naturally where the benefit of this method is. Nevertheless, the robustness and feasibility of this method never deteriorate because it is possible to compute the surface and estimated values in less than 10 seconds for the sparse data case based on the standard GP regression method.

Our method is the first to demonstrate that we can calculate the volume of TIHs accurately in real-time and use it as a measure of TIHs even when only a limited number of measurement points are available. In addition, the time series of the volumes obtained from the surface by points on the 80% and 99% one-sided confidence intervals (CIs) of the TEC values are also plotted in Figure 3.

The volume of the TIH begins to increase almost 10 minutes after the earthquake occurrence and continues to increase until about 28 minutes after the earthquake in Figure 3 (e) and (f). In this analysis, a provisional threshold is set at 200,000 TECu$\times$km^2. In the case of the full data, both panels show that the volumes calculated from the fitting surface (but not accounting for uncertainties in the approximation) reach the threshold 1 and 2 minutes earlier respectively than the volumes of 80% and 99% CI. Similarly, in the case of the sparse data, the time difference is about 2 and 4 minutes respectively to reach the threshold for the volumes computed from the fitting surface and both CIs. It means that thanks to our uncertainty computations, making sure that a warning is at a high level of confidence, based on data, of either 80% or 99% results in delays for advisories of only respectively 1-2 or 2-4 minutes.

4 Conclusion and Discussion

In this paper, we compute the volume of the ionospheric disturbance generated by a tsunami, in real time, and with enough confidence to issue warnings. The surface fits the TEC data using a Gaussian process regression after removing outliers. It enables us

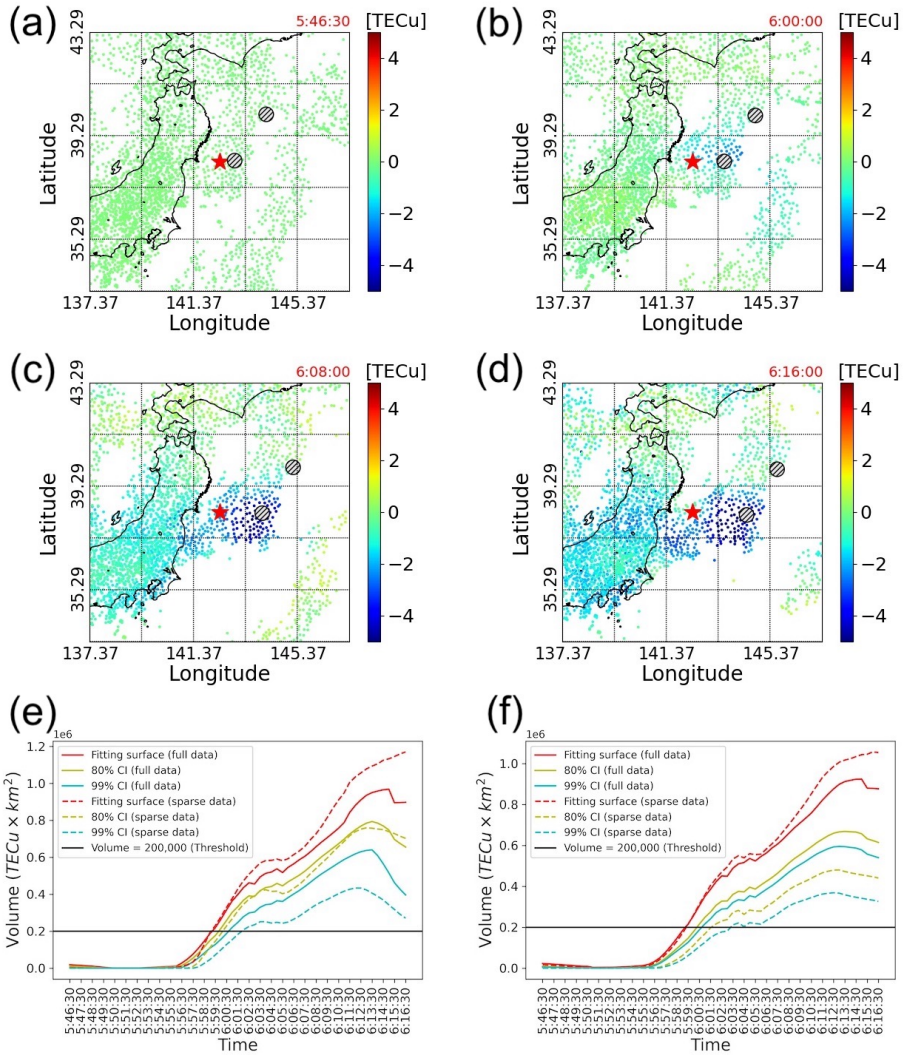

Figure 3. The top four panels are the observed data. The red star is the epicenter and the two large black circles are the outliers. The panel (a), (b), (c), and (d) are the TEC data measured at 5:46:30, 6:00:00, 6:08:00, and 6:16:00 UTC respectively. 5:46:30 was the time of the earthquake occurrence. The bottom two panels are the time series of TIH volume for full data and sparse data with one-sided confidence intervals. The red solid line is the volume calculated fitting surface with full data. The solid yellow line and the solid blue line are one-sided 80% CI and 99% CI respectively. The dashed lines are for sparse data with only 5% of receivers. The horizontal black line is a provisional threshold. Panel (e) is the TEC surface computed based on standard GP regression. Panel (f) is the TEC surface computed based on GP regression using the INLA-SPDE method.

to estimate the estimated TEC values over the entire target area. Furthermore, uncertainty can be properly evaluated for the estimated value of TEC according to the density of observations.

The TIH captured by our method is located east of the epicenter. This is consistent with the initial tsunami estimated by the inversion analysis of the waveforms being east of the epicenter (T. Saito et al., 2011). Also, the estimated TIH almost overlaps with the estimated initial tsunami area. In the ionosphere, the anisotropic conductance and geomagnetic field directions theoretically cause ionospheric currents to have complex shapes (Zettergren & Snively, 2019). We concretely show here that the estimated TIH can be anisotropic using observed TEC data and a statistical approach.

As shown in our results, this new method is robust as it works in situations where measurements are not uniformly distributed and moving, TIHs display anisotropy, and even if the number of observed data points is sparse. Since our estimates of the shape of the anisotropic TIHs reflect the signature of the initial tsunami wave, we demonstrate that using one specific data point such as the minimum observed value as a scale of a TIH is insufficient to characterise the initial wave. Our computation of the volume of TIHs as a measure to assess the scale of TIHs takes fully into account the spatial variations of the TEC depression generated by the tsunami over the domain, including any anisotropy.

As larger initial tsunamis cause larger decreases in TEC (Astafyeva et al., 2013; Kamogawa et al., 2016), if a TIH volume reaches a certain threshold, then it indicates that a large-scale initial tsunami has occurred. Therefore, using our method, it is possible to build an early warning system that issues a tsunami warning when the volume of the TIH exceeds a certain threshold, taking uncertainty into consideration. In our analysis, we set a provisional threshold at 200,000 TECu$\times$km^2, and it is clear that the volumes calculated using both full data and sparse data exceed the threshold within 15 minutes after the earthquake occurrence, or sooner with a lower threshold. Even carrying out the computations in the most exacting case, using 99% confidence intervals and sparse data (5% of the total observations) only delays the warning by around 4 minutes. We anticipate that more numerical work, more physical understanding of possible natural levels of TEC variations, and more data analysis will be required to establish more finely the thresholds at which advisories can be issued, and thus shorten the advisories to possibly 10 minutes or so. Our implementation on the 2011 Tohoku Earthquake in Japan

demonstrates that our method works well there. Hence it is very likely that this method can be applied to tsunamis around the world, caused by any kind of sources. This may enable the construction of a robust worldwide tsunami early warning system using the volume of TIHs as an index.

Acknowledgments

The authors acknowledge the use of the UCL Myriad High Performance Computing Facility (Myriad@UCL), and associated support services, in the completion of this work. RK is supported by the Japan Student Services Organization. This research was partly supported by the Ministry of Education, Science, Sports, and Culture through a Grant-in-Aid for Scientific Research (B) No. 17H02058, 2017-2020 (MK) and Earthquake Research Institute (University of Tokyo) cooperative research program (MK and RK). SG was supported by the Alan Turing Institute project "Uncertainty Quantification of complex computer models. Applications to tsunami and climate" under the EPSRC grant EP/N510129/1 and "Real-time Advanced Data assimilation for Digital Simulation of Numerical Twins on HPC" under the EPSRC grant EP/T001569/1.

Data Availability Statement: GPS data was provided by Geospatial Information Authority of Japan at `ftp://terras.gsi.go.jp/`. Currently, the data can be purchased from the Japan Association of Surveyors `http://www.jsurvey.jp/eng.htm`.

References

Astafyeva, E., Shalimov, S., Olshanskaya, E., & Lognonné, P. (2013). Ionospheric response to earthquakes of different magnitudes: Larger quakes perturb the ionosphere stronger and longer. *Geophysical Research Letters*, *40*(9), 1675–1681.

Chang, K.-L., Guillas, S., & Fioletov, V. (2015). Spatial mapping of ground-based observations of total ozone. *Atmospheric Measurement Techniques*, *8*(10), 4487–4505.

Cover, T., & Hart, P. (1967). Nearest neighbor pattern classification. *IEEE transactions on information theory*, *13*(1), 21–27.

Giles, D., Gopinathan, D., Guillas, S., & Dias, F. (2021). Faster than real time tsunami warning with associated hazard uncertainties. *Frontiers in Earth Science*, *8*, 560. Retrieved from `https://www.frontiersin.org/article/`

10.3389/feart.2020.597865 doi: 10.3389/feart.2020.597865

Kakinami, Y., Kamogawa, M., Tanioka, Y., Watanabe, S., Gusman, A. R., Liu, J.-Y., et al. (2012). Tsunamigenic ionospheric hole. *Geophysical Research Letters*, *39*(13).

Kamogawa, M., Orihara, Y., Tsurudome, C., Tomida, Y., Kanaya, T., Ikeda, D., et al. (2016). A possible space-based tsunami early warning system using observations of the tsunami ionospheric hole. *Scientific reports*, *6*, 37989.

Lay, T., Ammon, C. J., Kanamori, H., Yamazaki, Y., Cheung, K. F., & Hutko, A. R. (2011). The 25 october 2010 mentawai tsunami earthquake (mw 7.8) and the tsunami hazard presented by shallow megathrust ruptures. *Geophysical Research Letters*, *38*(6).

Lindgren, F., Rue, H., & Lindström, J. (2011). An explicit link between Gaussian fields and Gaussian Markov random fields: the stochastic partial differential equation approach. *Journal of the Royal Statistical Society: Series B (Statistical Methodology)*, *73*(4), 423–498.

Rue, H., Martino, S., & Chopin, N. (2009). Approximate Bayesian inference for latent Gaussian models by using integrated nested Laplace approximations. *Journal of the royal statistical society: Series b (statistical methodology)*, *71*(2), 319–392.

Saito, A., Tsugawa, T., Otsuka, Y., Nishioka, M., Iyemori, T., Matsumura, M., et al. (2011). Acoustic resonance and plasma depletion detected by GPS total electron content observation after the 2011 off the Pacific coast of Tohoku Earthquake. *Earth, planets and space*, *63*(7), 863–867.

Saito, T., Ito, Y., Inazu, D., & Hino, R. (2011). Tsunami source of the 2011 Tohoku-Oki earthquake, Japan: Inversion analysis based on dispersive tsunami simulations. *Geophysical Research Letters*, *38*(7).

Satake, K., Nishimura, Y., Putra, P. S., Gusman, A. R., Sunendar, H., Fujii, Y., ... Yulianto, E. (2013). Tsunami source of the 2010 mentawai, indonesia earthquake inferred from tsunami field survey and waveform modeling. *Pure and Applied Geophysics*, *170*(9-10), 1567–1582.

Shinagawa, H., Tsugawa, T., Matsumura, M., Iyemori, T., Saito, A., Maruyama, T., et al. (2013). Two-dimensional simulation of ionospheric variations in the vicinity of the epicenter of the Tohoku-oki earthquake on 11 March 2011.

Geophysical Research Letters, *40*(19), 5009–5013.

Tanioka, Y., & Gusman, A. R. (2018). Near-field tsunami inundation forecast method assimilating ocean bottom pressure data: A synthetic test for the 2011 tohoku-oki tsunami. *Physics of the Earth and Planetary Interiors*, *283*, 82–91.

Tsugawa, T., Saito, A., Otsuka, Y., Nishioka, M., Maruyama, T., Kato, H., et al. (2011). Ionospheric disturbances detected by GPS total electron content observation after the 2011 off the Pacific coast of Tohoku Earthquake. *Earth, planets and space*, *63*(7), 875–879.

Wang, Y., Maeda, T., Satake, K., Heidarzadeh, M., Su, H., Sheehan, A., & Gusman, A. (2019). Tsunami data assimilation without a dense observation network. *Geophysical Research Letters*, *46*(4), 2045–2053.

Williams, C. K., & Rasmussen, C. E. (2006). *Gaussian Processes for Machine Learning* (Vol. 2) (No. 3). MIT press Cambridge, MA.

Zettergren, M., & Snively, J. (2019). Latitude and Longitude Dependence of Ionospheric TEC and Magnetic Perturbations From Infrasonic-Acoustic Waves Generated by Strong Seismic Events. *Geophysical Research Letters*, *46*(3), 1132–1140.

Zettergren, M., Snively, J., Komjathy, A., & Verkhoglyadova, O. (2017). Nonlinear ionospheric responses to large-amplitude infrasonic-acoustic waves generated by undersea earthquakes. *Journal of Geophysical Research: Space Physics*, *122*(2), 2272–2291.